Nanoscale Advances

ROYAL SOCIETY OF CHEMISTRY

PAPER

View Article Online
View Journal | View Issue

Cite this: *Nanoscale Adv.*, 2023, **5**, 733

Cytotoxicity of mini gold nanorods: intersection with extracellular vesicles†

Ábner Magalhães Nunes,[ab] Priscila Falagan-Lotsch,[ac] Ayman Roslend,[a] Mario Roberto Meneghetti [b] and Catherine Jones Murphy [*a]

It is well-known that there are size- and shape-dependencies to nanoparticle uptake and processing by living cells. Small gold nanorods have shown to exhibit low toxicity and high clearance rates when compared to larger ones, making smaller particles more desirable for biomedical applications. In this study gold mini-rods (approximately 9.5 × 23, 8 × 26, and 6 × 26 nm, corresponding to aspect ratios 2.5, 3.2 and 4.1) and gold nanospheres (15.6 nm average diameter) were synthesized, and wrapped with cationic and anionic polyelectrolytes. This library of colloidally stable nanomaterials was exposed to human dermal fibroblasts at the relatively low concentration of 1 nM for each nanoparticle type. The cytotoxic profile of these nanoparticles and their influence on the small extracellular vesicles released by the cells was assessed. It was observed that although the nanoparticles were found in vesicles inside the cells, the cell viability, the mitochondrial membrane potential and levels of reactive oxygen species were not markedly affected by the mini gold nanorods. The production of extracellular vesicles by the cells was unaffected by gold nanoparticle exposure; moreover, no gold nanoparticles were observed in extracellular vesicles in the exosomal size range. Taken together, these results suggest that these mini gold nanorods are suitable for a wide range of cellular applications for relatively short-term studies.

Received 9th October 2022
Accepted 17th December 2022

DOI: 10.1039/d2na00694d

rsc.li/nanoscale-advances

Introduction

Nanomaterials have shown great promise for a wide range of applications.[1,2] The large use of these materials is mainly attributed to their unique physicochemical and optical properties which are different from their bulk form.[3] The properties of nanomaterials strongly depend on the size and shape of the nanoparticles (NPs).[4] Thus, by modifying the morphology and size of the nanoparticles, their properties can be tuned for specific applications.[5]

Notable progress has been made in modulating the size and shape of nanoparticles by the development of new synthetic methods. The Turkevich method is a traditional method for preparing nanospheres of gold.[6] For anisotropic gold nanoparticles, such as gold nanorods (AuNRs), seed-mediated methods have been developed, with well-established examples from our own group.[7] Recently, we reported the synthesis of "mini gold nanorods", with tunable longitudinal surface plasmon resonances, in high yield.[8] Due to their singular properties and features, AuNRs have been studied and directly applied for therapeutic purposes.[9] These nanoparticles present a characteristic, tunable absorption band from their surface plasmon resonances in the visible/near-infrared region, which is of great interest for biomedical applications such as biological imaging,[10] photothermal therapy,[11] biosensing[12] and drug[13]/gene[14] delivery.

Large particles (>50 nm) have shown to exhibit low cellular uptake and slow clearance,[15,16] making smaller particles, such as mini AuNRs, more desirable for biological studies. This might be explained assuming that large particles need to interact with a higher number of receptors, and they require higher energy to be internalized when compared to smaller ones.[17] Although the inner structure of the particles can strongly affect their properties, the surface chemistry plays an important role in their bioactivity and can directly affect cellular uptake, removal and toxicity.[18,19] Although several studies have shown the toxicity profile of different gold nanoparticles at different levels,[20–22] no data on mini gold nanorods have been reported thus far.

Recently, the incorporation of extracellular vesicle (EV) analyses in toxicological studies has been discussed. EVs are secreted by most types of cells[23] and have an important role in paracrine and autocrine cell communication by transferring

[a]*Department of Chemistry, University of Illinois at Urbana-Champaign, 600 S. Mathews Ave., Urbana, IL 61801, USA. E-mail: murphycj@illinois.edu*

[b]*Instituto de Química e Biotecnologia, Universidade Federal de Alagoas, Alagoas, 57072-900, Brazil*

[c]*Department of Biological Sciences, Auburn University, Auburn, Alabama 36849, USA*

† Electronic supplementary information (ESI) available: UV-vis spectra and DLS data of the particles after each polyelectrolyte coating layer. Study of the stability of the particles in cell media. Cell viability of HDF cells exposed to free PAA. Additional TEM micrographs of cells exposed to gold nanoparticles. Statistical analysis of the ratio green/red fluorescence on JC1 assay. Additional extracellular vesicles characterization. See DOI: https://doi.org/10.1039/d2na00694d

a wide variety of cargos (proteins, lipids, mRNA, or non-coding RNA such as miRNAs) through cells or tissues.[24,25] Studies have shown that external stressors such as exogenous chemicals may impact the secretion of EVs, modify their cargo, *etc.*[26–28] Exosomes are a subtype of EVs characterized by a size ranging between 50–150 nm[29] and they play a role in immune activation and in the pathogenesis and progression of various diseases. A recent study showed that the exposure of cells to 5 nm AuNPs can alter the biophysical characteristics of small EVs (<200 nm).[30] Moreover, since exosomes are formed in the endosomal pathway involving clathrin-coated vesicles,[31] one of the main endocytic pathways used by AuNPs for cellular internalization,[19] the uptake of these NPs by cells could potentially interfere in the small EVs synthesis and cargo sorting.

Incubating cells with nanoparticles is one of the strategies to produce EV-coated nanoparticles in order to facilitate their uptake by recipient cells, and to improve the efficacy and safety of synthetic nanoparticles as therapeutic and imaging agents.[33–35] However, investigations of how the nanoparticles can affect the production of the EV's remain scarce.

Therefore, in this present work we sought to assess the toxicity profile of mini AuNRs with different aspect ratios (ARs) in human dermal fibroblasts (HDF), a cell model in toxicological studies,[36–38] by evaluating cell viability, and mitochondrial parameters. We also examined the ability of mini gold nanorods to be excreted by these cells in small EVs, and how nanorod uptake by these cells influenced small EV production.

Experimental

Reagents and chemicals

Gold(III) chloride trihydrate ($HAuCl_4 \cdot 3H_2O$, ≥99.9%, Sigma-Aldrich), sodium borohydride ($NaBH_4$, >98%, Sigma-Aldrich), hexadecyltrimethylammonium bromide (CTAB, ≥99%, Sigma-Aldrich), sodium citrate (tribasic dehydrate, $C_6H_5Na_3O_7 \cdot 2H_2O$, ≥99%, Sigma-Aldrich), poly(allylamine hydrochloride) (PAH, M.W. 17,500 g mol^{-1}, Sigma-Aldrich), poly(acrylic acid) sodium salt (PAA, M.W. 15,000 g mol^{-1}, Sigma-Aldrich), silver nitrate ($AgNO_3$, 99.0%, Sigma-Aldrich), L-ascorbic acid (BioXtra, ≥99.0%, crystalline, Sigma-Aldrich), hydrochloric acid (HCl, certified 1.0 N, Fisher Chemical), phosphate-Buffer Saline (PBS, 1×, Corning), exosome-depleted FBS (Exo-FBS, SBI), trypan blue solution (0.4%, Invitrogen), Triton X-100 solution (BioUltra, Sigma-Aldrich), exosome precipitation kit (Exo-quick, SBI). All solutions were prepared with nanopure water.

Gold nanospheres preparation

Gold nanospheres (AuNSs) were synthesized *via* the Turkevich method.[6] In this method, citrate is used to reduce gold(III) ions to elemental gold in a gold chloride aqueous solution at 100 °C. For this, an aqueous solution of $HAuCl_4 \cdot 3H_2O$ was brought to a rolling boil under vigorous stirring. Then, 2 mL of 5 wt% aqueous solution of sodium citrate was added to the system. A solution color change from colorless to red was observed. After 30 minutes, 0.5 mL of 5 wt% sodium citrate was added and the mixture was heated for 10 more minutes. The solution was allowed to cool naturally. After synthesis, the AuNSs were centrifuged at 8000×*g* for 20 min and resuspended in water.

Mini gold nanorods preparation

Mini gold nanorods were synthesized as previously described by our group.[8] A seed solution was prepared by the addition of 0.25 mL of $HAuCl_4 \cdot 3H_2O$ (0.010 M) to 9.75 mL of CTAB (0.10 M). Then, 0.60 mL of ice-cold $NaBH_4$ solution (0.010 M) was added to the mixture with rapid stirring. The mixture was stirred for 10 minutes, and the final solution was left undisturbed at 27 °C for 1.5 h.

In a separate flask, a mixture of aqueous solutions of 0.5 mL of $HAuCl_4 \cdot 3H_2O$ (0.010 M), 8.0 mL of CTAB (0.10 M), and different amounts of 0.010 M $AgNO_3$ solution (0.030, 0.050 and 0.1 mL for the three different aspect ratios desired) was prepared. Then, 80 μL of freshly prepared ascorbic acid aqueous solution (0.10 M) was added. A change in the color of the solution from light yellowish to colorless can be observed. In the final step, 2 mL of seed solution were added to the growth solution and the mixture was rapidly stirred for 10 seconds and allowed to age overnight (16–20 h) at 27 °C. The solutions were centrifuged at 16 000×*g* for 35 min and resuspended in 1 mL of nanopure water.

Polyelectrolyte coating of gold nanoparticles

Both mini AuNRs and AuNSs were modified by sequential layer-by-layer polyelectrolyte coating.[39] First, 0.1 mL of 0.01 M NaCl was added to 1.0 mL the colloidal gold solution, followed by 0.2 mL of 10 mg mL^{-1} polymer solution (1 mM NaCl). The solution was left on a shaker for 2 hours, centrifuged at 16 000×*g* for 20 minutes and washed with nanopure water. This procedure was repeated three times using the sequence of polyelectrolytes PAA/PAH/PAA for AuNRs and PAH/PAA for AuNSs.

Colloidal analysis of the AuNPs

The colloidal gold nanoparticles were characterized by UV-vis spectroscopy (Cary 500 Scan UV-vis-NIR spectrophotometer, Varian), dynamic light scattering (DLS), transmission electron microscopy (TEM; 2100 JEOL Cryo TEM) and zeta potential measurements (ZetaPALS DLS/zeta potential analyzer, Malvern Instruments). The zeta potential measurements were performed on the colloids (0.5 nM) in nano pure water. For TEM analysis, the samples were prepared by adding a drop of the gold colloidal solution on a copper grid coated with a porous carbon film and were analyzed at an accelerating voltage of 200 kV.

Cell line and cell culture

Human dermal fibroblasts (HDF) cells (Sigma Aldrich) were cultured in T-75 flasks containing Dulbecco's modified eagle medium (DMEM, without phenol red), nonessential amino acids and 1% penicillin-streptomycin solution (Mediatech), along with 10% exosome-depleted FBS (Exo-FBS, SBI) in a humidified incubator with 5% CO_2 at 37 °C.

Cell viability

HDF cells (passage 05) were plated in triplicate into 24-well plates at 10 000 cells/well with 0.5 mL of cell media and were allowed to adhere to the plate overnight. The next day, the media was replaced with 0.5 mL of media containing 1 nM of gold nanoparticles (AuNPs). The concentration of 1 nM was chosen based on our previous studies using medium-sized AuNRs, which is concentrated enough that some effects may be observed, but not so concentrated that cell death occurs.[39] After 24 hours, the media was removed, and the cells were washed with PBS before the addition of 0.5 mL of AuNP-free media. At the time-points of 24, 48 and 72 hours after the AuNP incubation, the cells were trypsinized, centrifuged and resuspended in 100 μL of media. A mixture of cell suspension and 0.4% trypan blue solution (Invitrogen) was prepared for cell counting. The cells were manually counted in a hemocytometer counting chamber. Cells never exposed to media containing any type of AuNPs were used as controls.

Nanoparticle uptake

HDF cells were plated into 24-well plates at 10 000 cells/well with 0.5 mL of cell media and were allowed to adhere to the plate overnight. In the following day, the media in all samples (other than controls, which were just changed with AuNP-free media) was replaced with 0.5 mL of media containing 1 nm of AuNPs. After 24 hours, the media containing AuNPs was removed, and the cells were washed with PBS before adding 0.5 mL of AuNP-free media to each well. After 72 hours, the media was removed and the cells were washed with PBS, centrifuged, and resuspended in PBS for counting. Cells were then centrifuged again and resuspended in 1 mL of lysis buffer (2% Triton X-100 in PBS) and 1 mL of 30% hydrogen peroxide. A total of 3 mL of 70% nitric acid was added to each tube to dissolve any cell debris (overnight). The next day, 4 mL of fresh aqua regia were added to each tube to dissolve the gold (about 3 hours). After this time, 10 mL of ultrapure deionized water were added in the solution. The gold content in each sample was determined by inductively coupled plasma optical emission spectrometry (ICP-OES; PerkinElmer 2000DV ICP-OES) at the Mass Spectrometry Laboratory (University of South Carolina).

Confocal fluorescence microscopy

To evaluate mitochondrial toxicity (mitochondrial membrane potential and reactive oxygen species (ROS) production), confocal fluorescence microscopy was performed on HDF cells plated in 35 mm tissue culture dishes containing 14 mm glass bottom wells coated with poly-*d*-lysine (MatTek Corporation) at 10 000 cells/dish. The next day, the media was replaced with 2.0 mL of media containing 1 nM of gold nanoparticles (AuNPs). After 24 hours, the media was removed, and cells were washed with PBS before adding 2.0 mL of AuNP-free media to each dish.

To prepare the samples for imaging after 72 hours, the media was removed, and the cells were washed with 2.0 mL of HBSS. Then, 2.0 mL of the dye (JC-1 2.5 μg mL^{-1} or MitoSOX 5 μM) in OPTI-MEM were added to the dishes and incubated at 37 °C in the dark for 15 minutes. The cells were washed twice with 2.0 mL of HBSS followed by the addition of 2.0 mL of OPTI-MEM to the dishes. The cells were imaged with a Zeiss LSM 710 multiphoton confocal microscope with the laser power, gain, magnification, and all other parameters held constant. JC-1 and MitoSOX were evaluated as independent experiments.

Small extracellular vesicles purification and characterization

HDF cells cultured in T-75 flasks were allowed to grow until they achieved 90% confluency. The conditioned medium was then collected for small EVs isolation. Small EVs were purified by an Exo-quick exosome precipitation kit (SBI, Mountain View, CA) according to manufacturer instructions. Briefly, 10 mL of the conditioned medium were collected and centrifuged at 3000×*g* for 15 min. The supernatant was then transferred to a sterile centrifuge tube. A total of 2 mL of the Exo-Quick-TC solution were added to the medium, and the solution was mixed by inverting. The solution was left upright and stored in a refrigerator at 4 °C overnight. Then, the solution was centrifuged at 1500×*g* for 30 min. The supernatant was aspirated, and the pellet was centrifuged once again at 1500×*g* for 5 minutes to remove the residual precipitating solution. The final pellet was resuspended in 100 μL of PBS. Small EVs concentration and size were measured by Nanoparticle Tracking Analysis (Malvern NS300), and then, they were characterized by negative-staining TEM and biomarkers expression using Exo-Check Exosome Antibody Array (SBI, Mountain View, CA).

Nanoparticle tracking analysis

The concentration and the size of the small EVs isolated from the HDF cells were evaluated using nanoparticle tracking analysis (NTA) with the NanoSight NS300 (Malvern, UK). A total of 10 μL of the isolated small EVs were resuspended in 490 μL of PBS and loaded into the instrument at an infusion rate of 100 μL min^{-1} at 27 °C. A total of five 60 seconds videos were recorded and analyzed with the NTA 3.0 software (camera level 14; detection threshold 6). D10, D50 and D90 represent the maximum size of D% of the total sample.

Transmission electron microscopy

Prior to imaging, 20 μL of isolated small EVs were fixed with Karnovsky fixative (1 : 1). Then, 10 μL of the sample were loaded on top of a carbon-coated grid and left to dry for 30 minutes. The excess of sample was removed from the grid using a filter paper, and the grid was placed face-down on a drop of ammonium molybdate. The excess of ammonium molybdate was drained from the grids using a filter paper, and the grid was allowed to dry for 15 minutes before TEM imaging (Hitachi H600 TEM at 75 kV).

Total protein quantification

The protein content in isolated EVs was evaluated by the BCA Protein Assay Kit (ThermoFisher Scientific). For this, 100 μL of the isolated small EVs were added to a tube with 1.0 mL of the freshly made working reagent (0.1 M NaOH, sodium tartate,

sodium bicarbonate, sodium carbonate and copper sulfate). Then, the solution was incubated at 60 °C for 30 minutes, and the absorbance of the samples at 562 nm was measured after the solution has cooled to room temperature. The protein concentration was calculated based on a standard curve of BSA (1–250 μg mL^{-1}). All analyses were performed in triplicate.

Statistical analysis

One-way analysis of variance (ANOVA) followed by the Dunnett post hoc test was performed to examine differences between samples treated with AuNPs and controls. Data were expressed as the mean of three independent experiments (±standard deviation) and p-values <0.05 were considered to be statistically significant.

Results and discussion

In this study, we synthesized three different colloidal systems: mini gold nanorods (AuNRs) with three different aspect ratios (2.5, 3.2 and 4.1). As-made mini-rods presenting the well-known cytotoxic surfactant hexadecyltrimethylammonium bromide (CTAB) in their surfaces were coated with the polyelectrolytes poly(acrylic acid) (PAA) and poly(allylamine hydrochloride) (PAH) commonly used in nanomedicine applications, to eliminate the cytotoxicity associated with free CTAB.[39,40] Cell viability, AuNP uptake, mitochondrial membrane potential and reactive oxygen species levels were evaluated to provide a toxicity profile of the mini AuNRs in human dermal fibroblast cells, a commonly used non-transformed cell model in toxicology studies. The cytotoxicity of polyelectrolyte-coated spheres and uncoated CTAB mini gold nanorods (A.R. 2.5) were comparatively evaluated. In addition, we also investigated the potential impact of mini rods in the size, number and cargo of small EVs released by exposed HDF cells.

Gold nanoparticles synthesis

The as-made AuNPs were characterized by UV-vis-NIR spectroscopy and TEM. the UV-vis spectra for all mini nanorods are shown in Fig. 1a. The spectrum of the colloid containing spheres showed the typical extinction band relating to their single surface plasmon resonance. All colloids containing mini AuNRs showed two characteristic bands which are attributed to their transverse and longitudinal localized surface plasmon resonances (LSPR). The longitudinal plasmon band for the mini

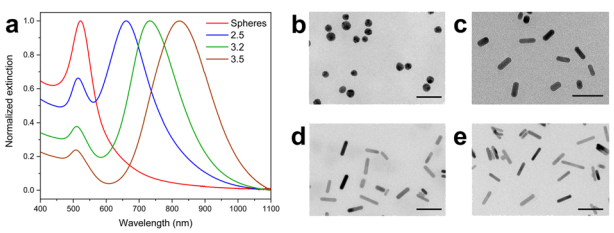

Fig. 1 UV-vis-NIR spectra of gold nanoparticles and TEM images of (b) spheres, and mini AuNRs of different aspect ratios: (c) 2.5, (d) 3.2 and (e) 4.1. Magnification 80kx (b) or 100kx (c, d and e), scale bars = 50 nm.

Table 1 Aspect ratios, plasmon maximum wavelengths, dimensions, and shape percent yield of the obtained systems

AR	SPR (nm)[a]	Length (nm)	Width (nm)	Shape (%)[c]
Spheres	526	15.6 ± 2.4[b]	—	97.8
2.5	661	23.3 ± 5.7	9.5 ± 1.9	95.3
3.2	734	25.7 ± 5.7	7.9 ± 1.4	93.9
4.1	833	26.0 ± 7.7	6.3 ± 1.2	94.7

[a] Longitudinal surface plasmon resonance (LSPR) for the rods. [b] Spheres' diameter. [c] $N = 250$ (80–100kx).

AuNRs varies depending on their aspect ratio (AR): the longitudinal band wavelengths were 661, 734, 833 nm for AR 2.5, 3.2, and 4.1 respectively. The redshift in the LSPR of the mini AuNRs is indicative of the increment in the AR, which is tuned by varying the concentration of $AgNO_3$ in the growth solution as previously reported.[8] The TEM data (Fig. 1b–e) was used to obtain the aspect ratios, dimensions, and shape percent yield for all systems (Table 1). The AuNSs showed a diameter of 15.6 nm and the mini AuNRs of different aspect ratios showed lengths ranging from 23.3 to 26.0 nm. Histograms showing the size distribution of all the particles are shown in Fig. S1.† The shape percent yield was calculated based on the obtained TEM images and was above 93.9% for all obtained systems.

Mini AuNRs surface modification

The presence of the CTAB in the synthesis of mini AuNRs is essential in the synthesis, as it forms a bilayer on the surface of the gold nanorods which aids in the anisotropic growth of the particles.[7] However, CTAB has shown to have toxic effects to cells.[41] In order to reduce the inherent toxicity of CTAB-capped AuNPs, all particles were washed and coated with three layers of polyelectrolytes (PAA/PAH/PAA). The use of these polyelectrolytes as coatings for gold nanoparticles have been extensively studied and have shown to possess good biocompatibility, especially PAA, which is the final layer for all systems.[39,40]

UV-vis-NIR spectra was taken after each step of coating (Fig. S3†). No significant changes were observed in the spectra of these particles besides a slight blueshift in the longitudinal band of the mini AuNRs, which may be associated with the interaction of PAA with the gold nanoparticle surface. The LSPR band of the AuNRs has been reported as extremely sensitive to changes in the size and aspect ratio of the particle as well as the dielectric constant of the capping agent on the particle surface.[42] These results show that all particles were stable during and after the polyelectrolyte coating process.

As part of AuNP characterization, the zeta potential of all systems was measured after each step of the coating procedure. Fig. 2 shows the changes in the zeta potential values as different polyelectrolyte layers were added to the particles. The inversion in the zeta potential values of the AuNPs suggests efficient coating after each sequence of polyelectrolyte addition. Mini AuNRs and the AuNSs showed negative zeta potentials in the final coating step with PAA. Additional data on the stability of

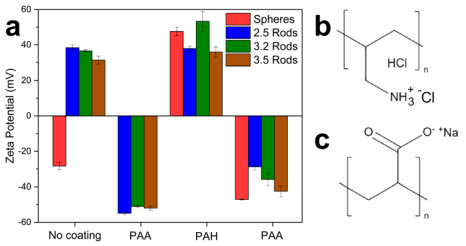

Fig. 2 (a) Zeta potential for each step of the polyelectrolyte-coating procedure for all gold nanoparticles. (b) Chemical structure of PAH. (c) Chemical structure of PAA.

the nanoparticles during the coating process are shown in Table S1.†

Mini AuNR uptake by HDF cells and intracellular localization

The amount of mini AuNRs ingested by the cells was evaluated by inductively coupled plasma optical emission spectroscopy (ICP-OES). Fig. 3a shows the average number of particles/cell after 72 hours. The results show that, with the exception of aspect ratio 3.2 mini-AuNRs, increased mini AuNR uptake is correlated with larger aspect ratio in this size range. Fernando and coworkers investigated the effect of the PEG-coated AuNRs of different AR in cellular uptake and showed that long AuNRs were internalized by HeLa cells to a greater extent when compared to shorter ones. However, the trend was not consistent for the smaller AR. In light of this, to establish the effect of AR on the endocytosis, other parameters such as, sedimentation, contact time, clustering, stability, internalization kinetic, and effect of bending energy should be also evaluated.[43]

To verify the localization of the gold nanoparticles inside the cells, the cells were exposed to the nanoparticles and whole-cell TEM images were taken. Fig. 3c–f show the TEM images of HDF cells incubated with different AuNPs at 1.0 nM after 72 hours. The examination of these images revealed that the

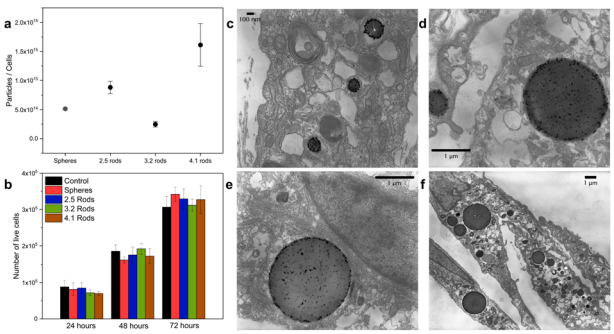

Fig. 3 (a) Average number of NPs per cell measured by ICP-OES analysis for gold content after 72 hours, (b) viability of HDF cells exposed to 1.0 nM of polyelectrolyte-coated mini AuNRs (2.5, 3.2 and 4.1) and polyelectrolyte-coated AuNSs, and transmission electron micrographs of the interior HDF cells 72 hours after exposure to 1.0 nM (c) AuNSs and different aspect ratio mini gold nanorods: (c) 2.5 rods, (d) 3.2 rods and (e) 4.1 rods. Data were analysed by one-way analysis of variance (ANOVA) followed by the Dunnett post hoc test, and $p < 0.05$ was considered statistically significant, $n = 4$.

nanoparticles were found inside endosomes/lysosomes of the cells. This is indicative of the internalization of the AuNPs *via* the endocytic pathway, which has been previously reported for other AuNPs.[19,32] AuNPs are directly coated with the plasma proteins when exposed to physiological solutions; internalization is mainly through clathrin- and caveolae-mediated endocytosis pathways.[19] No particles were found free in the cytoplasm in the first 72 hours of the experiment, indicating that these particles may be removed from the cells by vesicle-mediated exocytosis.

PAA-coated mini AuNRs are not toxic to HDF cells

Cell viability assays were performed on the anionic triple-wrapped mini AuNRs with the cells. Human dermal fibroblasts (HDF) were exposed to 1.0 nM of the polyelectrolyte-coated mini AuNRs for 24, 48, and 72 hours (Fig. 3b). Human skin cells are potentially a model for skin toxicity.[44] HDF cells, in particular, have been widely used as a model for toxicity studies using different nanomaterials.[37,38] Prior to the exposure, the colloidal stability of all polyelectrolyte-coated AuNPs in cell culture media was assessed; no aggregation was observed for all AuNPs suspensions (Fig. S4†). No significant changes were found in the number of live cells for all the systems studied when compared to the cells in the absence of nanoparticles (controls) (Fig. 3b). This indicates that under these experimental conditions, the polyelectrolyte-coated mini AuNRs showed good biocompatibility.

The fact that our data did not show a significant loss of cell viability demonstrates that these anionic gold NPs are reasonably safe materials. It has been reported that coating the original CTAB-AuNRs with polyelectrolytes, such as PAH and PAA, decreases their toxicity to cells by retarding the desorption of the CTAB molecules from the surface of the AuNRs.[38] Additionally, we investigated the toxicity effect of free PAA (the final coating layer of polyelectrolyte) on HDF cells (Fig. S5†). We estimated that the concentration of PAA in the final colloidal solution is less than 10 μM and at this concentration, no loss in cell viability was found.

Although a great amount of gold nanoparticles was found inside the cells no significant changes in the cell viability was observed. To provide a more comprehensive view of the changes in the behavior of the cell that may be induced by AuNPs exposure, we investigated some intracellular parameters related to cellular stress.

PAA-coated mini AuNRs do not disrupt mitochondrial activity nor induce mitochondrial stress

Mitochondria are critical for maintaining cellular homeostasis. The mitochondrial membrane electrochemical potential (MMP) is generated in the mitochondria due to the constant pumping of protons from the mitochondrial matrix to the intermembrane space in response to the flux of electrons from the catabolic processes. The maintenance of this potential is essential for the synthesis of the majority of ATP in eukaryotic cells. Thus, any change in the MMP can lead to cell death.[45] In this study, we used the mitochondrion-specific dye JC-1 to detect changes in

the mitochondrial membrane potential. JC-1 is a cationic dye that exhibits a potential-dependent accumulation in the mitochondria. The potential-sensitive color shift from green to red when J-aggregates are formed in the energized mitochondria. Therefore, the loss of the mitochondrial membrane potential is observed when the ratio of green/red fluorescence is increased. The presence of the polyelectrolyte-coated gold nanoparticles did not induce mitochondrial damage in the cells, as the JC-1 fluorescence remains similar to the controls (Fig. 4). The quantification data of MMP in HDF cells exposed to AuNPs can be found in Fig. S7.† Mini AuNRs showed similar data when compared to spheres. To evaluate the effectiveness of the polyelectrolyte coating, we also verified the effect of non-coated CTAB-rods (AR 2.5). In contrast to the PAA-coated mini AuNRs samples, the presence of CTAB in the surface of non-coated AuNRs increased the green fluorescence, which indicates the loss in the mitochondrial membrane potential. The ratio green/red fluorescence in Fig. S5† shows that there are no significant changes in this parameter for all the polyelectrolyte-coated AuNPs, suggesting that they did not impact the cellular metabolism *via* the mitochondrial pathway.

It has been shown that positively-charged CTAB-rods are electrostatically attracted to the mitochondria in response to the negative internal transmembrane potentials and can easily overcome the mitochondrial hydrophobic barriers, disrupting the electrochemical potential.[46] This may explain the distinct behavior for this specific system.

Mitochondria are the main source of reactive oxygen species (ROS) production. These species are generated as a product of metabolism. It is well-known that high doses of ROS are harmful for cells since ROS accumulation can induce oxidative stress leading to cell injury.[47] Oxidative stress represents a major initiator of the adverse biological outcomes of engineered nanomaterials. To assess the potential of mini AuNRs to induce the production of reactive oxygen species, the levels of superoxide produced by mitochondria in cells exposed to such NPs were evaluated (Fig. 5). The level of ROS was not significantly affected in HDF cells exposed to polyelectrolyte-coated mini AuNRs, nor AuNSs. However, the cells exposed to as-made CTAB-rods showed a significant increase in the

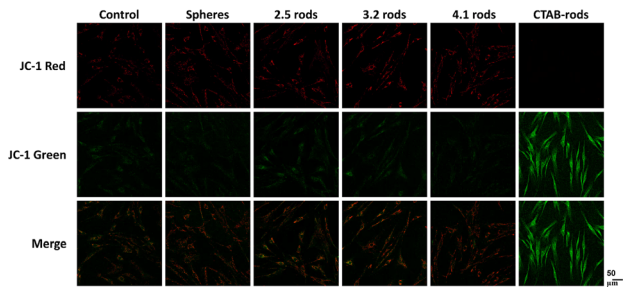

Fig. 4 The effect of different polyelectrolyte-coated mini gold nanorods in the mitochondrial membrane potential (MMP) of HDF cells measured by JC1 dye. Representative fluorescence images of HDF cells in the presence of absence of gold nanoparticles. CTAB-rods (AR 2.5) were used to assess the effect of non-coated AuNRs in MMP, $n = 3$.

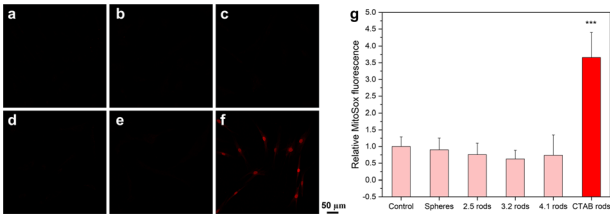

Fig. 5 The effect of different polyelectrolyte-coated gold nanoparticles in the mitochondrial superoxide production of HDF cells. Representative images of MitoSOX red staining of superoxide radicals in (a) HDF cells with no treatment, HDF cells exposed to 1.0 nM of (b) spheres and different aspect ratio mini gold nanorods: (c) 2.5 rods, (d) 3.2 rods and (e) 4.1 rods; and (f) uncoated CTAB-rods (A.R. 2.5). (g) Quantitative fluorescence intensity analyzed by ImageJ software. Data are represented as means of three independent experiments.

superoxide levels (Fig. 5f). The inert effect of the PAA-coated AuNPs in the mitochondrial membrane potential and in the superoxide level shows that although the particles are inside the cells, they are not provoking oxidative stress.

Therefore, our data demonstrated that the anionic, polyelectrolyte-wrapped mini AuNRs did not affect cell viability and metabolism beyond the controls.

Effect of mini AuNRs in the small EVs size, concentration, and cargo

In the recent years, EVs have emerged as a powerful mediator of environmental stimuli to and between cells. Analysis of EVs has been recognized as an important tool to investigate the potential of environmental stressors to cause deleterious impact on cell physiology.[27] To evaluate the impact of mini AuNRs on the EVs release and cargo, small EVs were isolated from conditioned cell culture media of HDF cells (Fig. S8†) that were exposed to mini AuNRs of different aspect ratios for 72 h. At the day of exposure, the cell media incubated with AuNPs showed a slightly dark color due to the high concentration of particles in the media (1.0 nM). On the other hand, during the small EVs isolation from the cell media after 72 hours, no color was observed.

The typical exosome morphology (bilayer membrane vesicles) was observed in transmission electron microscopy (TEM) images (Fig. 6e). The negative-stained TEM of small EVs shows their typical cup-shaped morphology for all the groups (Fig. 6e–i). Recent studies demonstrate that EVs is the pathway used by certain AuNPs to be cleared from cells.[33–35,48] Folic acid-conjugated PEG-AuNPs were shown to be incorporated by B16F10 cells *via* endocytosis and subsequently released as cargos inside EVs.[34] PEGylated hollow gold nanoparticles were also found to be loaded within EVs secreted by MSCs cells.[49] Alkylated (dodecyl-terminated, PEG-coated AuNPs) gold nanoparticles were also found to be accumulated inside EVs. This study showed that the pathway for the exocytosis of the EVs that are secreted alongside the exocytosed AuNPs depends on dodecyl loading. The increase on the alkyl percentage on the dodecyl-terminated PEG-AuNPs was able to promote an increase on their accumulation inside EVs.[48] On the other hand,

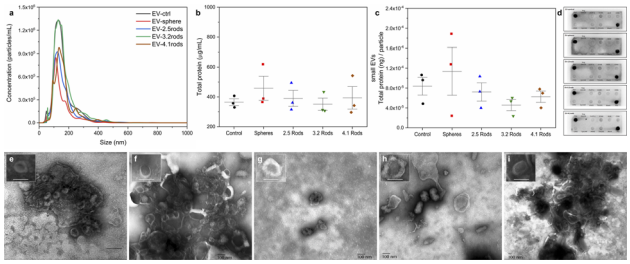

Fig. 6 Effect of AuNPs in the small EVs released by HDF cells. (a) Size distribution of the EVs isolated from cells exposed to gold nanoparticles. (b) Total protein concentration in EVs samples of cells exposed to gold nanoparticles, $n = 3$. (c) Correlation between protein contents and particle concentrations. (d) Exo-Check exosome antibody array for exosomal protein marker detection and assessment of cellular contamination. TEM images of extracellular vesicles released by cells exposed to gold nanoparticles: (e) EV-control, (f) EV-2.5 rods, (g) EV-3.2 rods and (h) EV-4.1 rods. Data were analysed by one-way analysis of variance (ANOVA) followed by the Dunnett post hoc test, and $p < 0.05$ was considered statistically significant, $n = 3$.

another study also performed the direct incubation of cells with a medium containing gold nanoparticles (citrate-capped AuNPs), and no data on particles inside EVs were reported.[30] It is well known that the surface chemistry of AuNPs mediates their exocytosis in different cells.[19] In our study, no polyelectrolyte-wrapped AuNP was found into the small EVs, as judged by TEM micrographs. Moreover, ICP-OES analysis was performed to confirm that our mini gold nanorods were not present in the EVs released by HDF cells. Additionally, the identity of the EVs was confirmed using Exo-Check antibody array which detects exosome biomarkers. Fig. 6d reveals the presence of transmembrane proteins (FLOT-1, ICAM, CD63 and CD81) and cytosolic proteins (TSG101, ANXA5 and ALIX) for all groups. In addition, no detection was seen for a *cis*-Golgi marker (GM130), a negative protein marker. According to the International Society for Extracellular Vesicles,[23] in order to validate the presence of EVs, the general protein characterization should include at least three positive protein markers, including at least one transmembrane and cytosolic protein and at least one negative protein marker. Based on nanoparticle tracking analysis (NTA) results, the average of the mode size for small EVs derived from HDF cells treated with different mini AuNRs were: EV-control 128.3 ± 5.1 nm; EV-spheres 134.9 ± 16.1 nm; EV-2.5 rods 125.1 ± 1.5 nm; EV-3.2 rods 123.5 ± 11.3 nm; EV-4.1 rods 134.0 ± 14.8 nm (Fig. 6a). None of the treatments with mini AuNRs impacted the size of the small EVs isolated from HDF exposed cells compared to controls and treatment with spheres. These data proved a successful isolation of small EVs derived from HDF cells.

The EVs showed a hydrodynamic size in a range of 123 to 139 nm and the concentrations were all above 3.0×109 particles per mL. A recent study showed that isolated EVs from mouse embryonic stem cells (mESCs) exposed to gold nanospheres (5 μg mL^{-1}) ranging from 5 to 80 nm presented similar sizes.[30]

To evaluate a potential interference of the presence of AuNRs in HDF cells in the cargo, the total protein content in each small EVs sample was evaluated by the BCA assay. As shown in Fig. 6b, we did not observe significant changes in the total protein in EVs isolated from cells exposed to any AuNPs. In addition, all systems presented in Fig. 6c showed similar correlation between the protein concentration and the small EVs particle concentration. Our data suggests that the presence of the AuNPs in these cell does not provoke significative disturbance in the amount of released EVs or their total protein content. Hao *et al.* showed that EVs released by cells exposed to 5 nm citrate-spheres (5 μg mL^{-1}) present equal protein content when compared to control EVs.[30] Another study demonstrated that hollow gold nanoparticles (125 μg mL^{-1}) do not significantly alter EVs structure, morphology, or expression of specific proteins.[49]

Conclusions

In this study we synthesized mini gold nanorods of different aspect ratios (2.5, 3.2, 4.1) to evaluate their toxicity profile towards HDF cells. The particles obtained were successfully coated with polyelectrolytes and demonstrated to be stable in cell media and nontoxic for HDF cells at the concentration of 1.0 nM. The TEM images of the cells showed that all the AuNPs were found inside vesicles in the cells which suggests the endocytic pathway in which the AuNPs are internalized by the cells. Even at this concentration, mini AuNRs did not affected significantly the mitochondrial electrochemical potential and ROS production, showing similar behavior to the spheres.

Our data also showed that the gold nanoparticles used in this study did not affect the profile of the small EVs released by the HDF cells. The characterization of the small EVs isolated from cells exposed to AuNPs revealed no significant changes in the total protein concentration. In addition, the concentration of particles evaluated by NTA were found similar for all the groups studied, suggesting that these particles might be processed by the cells in a manner that does not interfere with exosome pathways. From this data, we see that polyelectrolyte-coated mini gold nanorods did not show significative effect on cell and EVs in all the parameters evaluated which makes them highly promising for biomedical applications. Our data do not support the idea that our NPs could interfere with cellular signaling *via* exosome disruption, as other studies have shown for different NPs. Therefore, the NPs described here, which can be measured by many methods in a cellular context, show excellent biocompatibility and can serve as "neutral observers" of cellular events *via* various forms of microscopy and spectroscopy, or as photothermal heaters to cause light-triggered changes in cells with no NP background.

Conflicts of interest

There are no conflicts to declare.

Acknowledgements

We thank Sandra Key McMasters of the School of Chemical Science Cell Media Facility for expert assistance with cell

culture; Dr Lou Ann Miller of the Frederick Seitz Materials Research Laboratory for transmission electron microscopy data of cells; and the staff of the University of South Carolina's Department of Chemistry and Biochemistry Mass Spectrometry Laboratory. This work was supported by the National Institutes of Health (GM125845). A. M. N. thanks the National Counsel of Technological and Scientific Development (CNPq) and the Coordination for the Improvement of Higher-Level Education (CAPES) from Brazil for funding.

References

1 Y. Wu, M. R. K. Ali, K. Chen, N. Fang and M. A. El-Sayed, *Nano Today*, 2019, **24**, 120–140.
2 J.-H. Lee, H.-Y. Cho, H. K. Choi, J.-Y. Lee and J.-W. Choi, *Int. J. Mol. Sci.*, 2018, **19**, 1–14.
3 H. Chen, K. Zhou and G. Zhao, *Trends Food Sci. Technol.*, 2018, **78**, 83–94.
4 C. J. Orendorff, T. K. Sau and C. J. Murphy, *Small*, 2006, **2**, 636–639.
5 I. Khan, K. Saeed and I. Khan, *Arabian J. Chem.*, 2019, **12**, 908–931.
6 J. Turkevich, P. C. Stevenson and J. Hillier, *J. Phys. Chem.*, 1953, **57**, 670–673.
7 N. R. Jana, L. Gearheart and C. J. Murphy, *J. Phys. Chem. B*, 2001, **105**, 4065–4067.
8 H.-H. Chang and C. J. Murphy, *Chem. Mater.*, 2018, **30**, 1427–1435.
9 M. R. K. Ali, Y. Wu and M. A. El-Sayed, *J. Phys. Chem. C*, 2019, **123**, 15375–15393.
10 Y.-S. Chen, Y. Zhao, S. J. Yoon, S. S. Gambhir and S. Emelianov, *Nat. Nanotechnol.*, 2019, **14**, 465–472.
11 B. Zhou, J. Song, M. Wang, X. Wang, J. Wang, E. W. Howard, F. Zhou, J. Qu and W. R. Chen, *Nanoscale*, 2018, **10**, 21640–21647.
12 S. K. Maji, *ACS Appl. Nano Mater.*, 2019, **2**, 7162–7169.
13 Z. Song, Y. Liu, J. Shi, T. Ma, Z. Zhang, H. Ma and S. Cao, *Mater. Sci. Eng., C*, 2018, **83**, 90–98.
14 H. Nakatsuji, K. Kawabata Galbraith, J. Kurisu, H. Imahori, T. Murakami and M. Kengaku, *Sci. Rep.*, 2017, **7**, 4694.
15 B. D. Chithrani, A. A. Ghazani and W. C. W. Chan, *Nano Lett.*, 2006, **6**, 662–668.
16 Z. Li, S. Tang, B. Wang, Y. Li, H. Huang, H. Wang, P. Li, C. Li, P. K. Chu and X.-F. Yu, *ACS Biomater. Sci. Eng.*, 2016, **2**, 789–797.
17 C. Carnovale, G. Bryant, R. Shukla and V. Bansal, *ACS Omega*, 2019, **4**, 242–256.
18 N. Lewinski, V. Colvin and R. Drezek, *Small*, 2008, **4**, 26–49.
19 N. Oh and J.-H. Park, *ACS Nano*, 2014, **8**, 6232–6241.
20 K. Choi, J. E. Riviere and N. A. Monteiro-Riviere, *Nanotoxicology*, 2017, **11**, 64–75.
21 Y.-P. Jia, B.-Y. Ma, X.-W. Wei and Z.-Y. Qian, *Chin. Chem. Lett.*, 2017, **28**, 691–702.
22 Á. M. Nunes, K. R. M. da Silva, C. M. S. Calado, K. L. A. Saraiva, R. C. B. Q Figueiredo, A. C. R. Leite and M. R. Meneghetti, *Toxicology*, 2019, **413**, 24–32.
23 C. Théry, K. W. Witwer, E. Aikawa, M. J. Alcaraz, J. D. Anderson, R. Andriantsitohaina, *et al.*, *J. Extracell. Vesicles*, 2018, **7**, 1535750.
24 R. J. Lobb, M. Becker, S. W. Wen, C. S. F. Wong, A. P. Wiegmans, A. Leimgruber and A. Möller, *J. Extracell. Vesicles*, 2015, **4**, 27031.
25 G. Raposo and P. D. Stahl, *Nat. Rev. Mol. Cell Biol.*, 2019, **20**, 509–510.
26 E. Chiaradia, B. Tancini, C. Emiliani, F. Delo, R. M. Pellegrino, A. Tognoloni, L. Urbanelli and S. Buratta, *Cells*, 2021, **10**, 1763.
27 J. Ye and X. Liu, *Front. Immunol.*, 2022, **13**, 955419.
28 Q. Wu, H. Zhang, S. Sun, L. Wang and S. Sun, *Cell Death Dis.*, 2021, **12**, 894.
29 T. Cloet, N. Momenbeitollahi and H. Li, *Anal. Biochem.*, 2021, **622**, 114168.
30 F. Hao, T. Ku, X. Yang, Q. S. Liu, X. Zhao, F. Faiola, Q. Zhou and G. Jiang, *Nanoscale*, 2020, **12**, 15631–15637.
31 J. Lötvall, A. F. Hill, F. Hochberg, E. I. Buzás, D. Di Vizio, C. Gardiner, Y. S. Gho, I. V. Kurochkin, S. Mathivanan, P. Quesenberry, S. Sahoo, H. Tahara, M. H. Wauben, K. W. Witwer and C. Théry, *J. Extracell. Vesicles*, 2014, **3**, 26913.
32 C. Roma-Rodrigues, L. R. Raposo, R. Cabral, F. Paradinha, P. V. Baptista and A. R. Fernandes, *Int. J. Mol. Sci.*, 2017, **18**, 162.
33 P. Fathi, L. Rao and X. Chen, *View*, 2021, **2**, 20200187.
34 P. Lara, S. Palma-Florez, E. Salas-Huenuleo, I. Polakovicova, S. Guerrero, L. Lobos-Gonzalez, A. Campos, L. Muñoz, C. Jorquera-Cordero, M. Varas-Godoy, J. Cancino, E. Arias, J. Villegas, L. J. Cruz, F. Albericio, E. Araya, A. H. Corvalan, A. F. G. Quest and M. J. Kogan, *J. Nanobiotechnol.*, 2020, **18**, 20.
35 U. Kauscher, J. Penders, A. Nagelkerke, M. N. Holme, V. Nele, L. Massi, S. Gopal, T. E. Whittaker and M. M. Stevens, *Langmuir*, 2020, **36**, 3912–3923.
36 R. Romeo, M. A. Chiacchio, A. Campisi, G. Monciino, L. Veltri, D. Iannazzo, G. Broggini and S. V. Giofrè, *Molecules*, 2018, **23**, 1754.
37 Y. Huang, X. Lü and J. Ma, *J. Biomed. Nanotechnol.*, 2014, **10**, 3304–3317.
38 J. A. Yang, S. E. Lohse and C. J. Murphy, *Small*, 2014, **10**, 1642–1651.
39 P. Falagan-Lotsch, E. M. Grzincic and C. J. Murphy, *Proc. Natl. Acad. Sci. U. S. A.*, 2016, **113**, 13318–13323.
40 A. M. Alkilany, P. K. Nagaria, C. R. Hexel, T. J. Shaw, C. J. Murphy and M. D. Wyatt, *Small*, 2009, **5**, 701–708.
41 A. M. Alkilany, S. E. Lohse and C. J. Murphy, *Acc. Chem. Res.*, 2013, **46**, 650–661.
42 S. Eustis and M. A. El-Sayed, *Chem. Soc. Rev.*, 2006, **35**, 209–217.
43 D. Fernando, S. Sulthana and Y. Vasquez, *ACS Appl. Bio Mater.*, 2020, **3**, 1374–1384.
44 J. K. Lee, D. B. Kim, J. I. Kim and P. Y. Kim, *Toxicol. In Vitro*, 2000, **14**, 345–349.
45 P. J. Burke, *Trends Cancer*, 2017, **3**, 857–870.

46 L. Wang, Y. Liu, W. Li, X. Jiang, Y. Ji, X. Wu, L. Xu, Y. Qiu, K. Zhao, T. Wei, Y. Li, Y. Zhao and C. Chen, *Nano Lett.*, 2011, **11**, 772–780.
47 V. J. Thannickal and B. L. Fanburg, *Am. J. Physiol.: Lung Cell. Mol. Physiol.*, 2000, **279**, L1005–L1028.
48 L. W. C. Ho, C. K. W. Chan, R. Han, Y. F. Y. Lau, H. Li, Y.-P. Ho, X. Zhuang and C. H. J. Choi, *ACS Nano*, 2022, **16**, 2032–2045.
49 M. Sancho-Albero, N. Navascués, G. Mendoza, V. Sebastián, M. Arruebo, P. Martín-Duque and J. Santamaría, *J. Nanobiotechnol.*, 2019, **17**, 16.